Dual Passivation of Intrinsic Defects at the Compound Semiconductor/Oxide Interface Using an Oxidant and a Reductant

Tyler Kent,[†] Evgeniy Chagarov,[‡] Mary Edmonds,[†] Ravi Droopad,[§] and Andrew C. Kummel[*,†,‡]

[†]Materials Science and Engineering Department and [‡]Department of Chemistry and Biochemistry, University of California San Diego La Jolla, California 92093-0332, United States and [§]Department of Physics, Texas State University San Marcos, Texas 78666, United States

ABSTRACT Studies have shown that metal oxide semiconductor field-effect transistors fabricated utilizing compound semiconductors as the channel are limited in their electrical performance. This is attributed to imperfections at the semiconductor/oxide interface which cause electronic trap states, resulting in inefficient modulation of the Fermi level. The physical origin of these states is still debated mainly because of the difficulty in assigning a particular electronic state to a specific physical defect. To gain insight into the exact source of the electronic trap states, density functional theory was employed to model the intrinsic physical defects on the InGaAs (2 × 4) surface and to model the effective passivation of these defects by utilizing both an oxidant and a reductant to eliminate metallic bonds and dangling-bond-induced strain at the interface. Scanning tunneling microscopy and spectroscopy were employed to experimentally determine the physical and electronic defects and to verify the effectiveness of dual passivation with an oxidant and a reductant. While subsurface chemisorption of oxidants on compound semiconductor substrates can be detrimental, it has been shown theoretically and experimentally that oxidants are critical to removing metallic defects at oxide/compound semiconductor interfaces present in nanoscale channels, oxides, and other nanostructures.

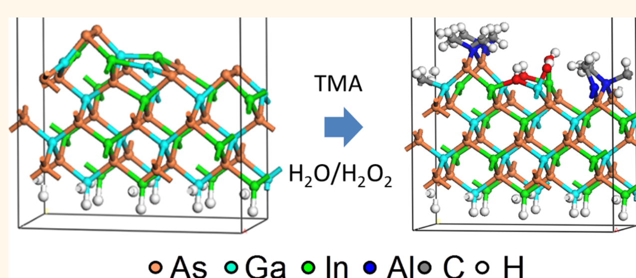

KEYWORDS: InGaAs · interface · passivation · aluminum oxide · MOSFET · Fermi level unpinning

Traditional metal oxide semiconductor field-effect transistors (MOSFETs) utilized Si as the channel material, but in an effort to increase processing power in logic devices, compound semiconductors are being explored as an alternative channel due to their intrinsically high mobilities.[1,2] Studies over the past several decades have concluded that a limiting factor to compound semiconductor-based MOSFET performance is the large density of interface trap states at the semiconductor/oxide interface.[3−7] These electronic trap states are hypothesized to be a result of physical imperfections at the semiconductor/oxide interface such as dangling bonds, highly strained bond angles, and metallic bonds, although this is still a topic of debate.[8,9] In order to develop effective passivation techniques for compound semiconductor/oxide interfaces, it is critical to definitively identify the physical origin of these electronic trap states. Previous work has shown that the deposition of a-Al_2O_3 on the InGaAs (2 × 4) surface results in promising capacitance voltage (CV) characteristics.[10] Therefore, the As-rich (2 × 4) reconstruction of InGaAs is a viable choice for use as a surface channel, but there is a fundamental problem with this surface for alloy compositions ranging from InAs to GaAs.

Edmonds *et al.* showed that GaAs (2 × 4) or InAs (2 × 4) surfaces contain at least 8% α2-(2 × 4) unit cells, and $In_{0.53}Ga_{0.47}As$ contains 71% α2-(2 × 4) unit cells, which accentuates the need to effectively passivate these defect unit cells.[11] The α2-(2 × 4) unit cell is missing an As−As dimer on the row, which results in metallic In−Ga bonds.[12] The metal−metal bonds directly form valence band (VB) edge states and indirectly induce conduction band (CB) edge

* Address correspondence to akummel@ucsd.edu.

Received for review November 4, 2014 and accepted April 6, 2015.

Published online April 06, 2015
10.1021/nn5063003

© 2015 American Chemical Society

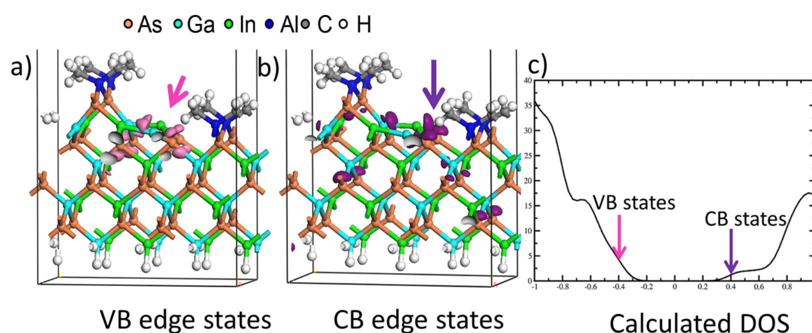

Figure 1. (a) Side view of relaxed DFT models of TMA passivated α2-(2 × 4) unit cell, with pink lobes showing the origin of VB edge states. (b) Purple lobes showing the origin of CB edge states. (c) Density of states of the TMA passivated α2-(2 × 4) unit cell, with arrows indicating the band edge states.

states; the metal−metal bonds generate bond angle strain in the edge As atoms which prefer to be in a tetrahedral sp^3 bonding configuration. This bond strain results in CB edge states as seen in density functional theory (DFT) calculations of the (2 × 4) surface density of states (DOS) and prevents the Fermi level (E_f) from being efficiently modulated without proper passivation techniques. Therefore, the InGaAs (2 × 4) reconstruction requires passivation of at least three unique sites: As dangling bonds, In/Ga dangling bonds, and In/Ga−In/Ga bonds.

Many passivation techniques have been explored for compound semiconductor surfaces, but most rely on external wet cleans, chemicals that are not ideal for introduction into commercial atomic layer deposition (ALD) tools, or temperatures that are not practical.[13−17] Another option would be to avoid the inherent problems of the InGaAs (2 × 4) surface by using another crystallographic face such as the (110) surface, which is defect-free.[18−20] While predosing with a reductant such as trimethylaluminum (TMA) is well-known to improve device characteristics and reduce native oxides,[10,21] the reductant (TMA) can only passivate the dangling bonds on the As atoms since bonding to a metal (Al) cannot passivate either In/Ga dangling bonds or In/Ga−In/Ga metallic bonds.[22] To improve III−V (2 × 4)-based MOSFET device performance, it may be possible to passivate the high density of defect unit cells using *in situ* chemical processes which preferentially insert an oxidant species such as an −OH group into the metallic bonds and relieve the strained As bonds. In this work, a passivation technique which utilizes a reductant (TMA) and an oxidant (OH, SH, NH_2) to passivate defect unit cells on the InGaAs (001)-(2 × 4) surface is modeled using DFT and experimentally tested using scanning tunneling microscopy and spectroscopy (STM, STS). To determine the chemical mechanism of passivation, the order of TMA/oxidant dosing was reversed and two different oxidants were studied.

RESULTS AND DISCUSSION

Density Functional Theory Simulations. Figure 1 shows a DFT model of the InGaAs (001) α2-(2 × 4) defect unit cell with a missing As row dimer which had been passivated with a full monolayer of dimethylaluminum (DMA). In the calculated DOS (c), small VB and CB edge states are observed, pink and purple arrows, respectively. The band decomposed charge density (left and middle) shows the origin of these states in the structural models. Figure 1a shows the VB edge states (pink lobes) that are predominantly concentrated on the In−Ga metallic bonds. Figure 1b shows that the CB edge states (purple lobes) originate mainly from the edge sp^3-hybridized As atoms that have a highly strained bond angle of about 65°, which is much smaller than the ideal tetrahedral angle of 109.5°.

To model the effects of oxidant passivation, calculations were performed for −O−, −S−, and −NH insertion into the metallic group III bonds to eliminate the metal−metal bonds and relieve the strained As bonds. Figure 2 shows the resulting bonding configurations and calculated DOS after oxidant insertion. The electronic structures for −O−, −S−, and −NH insertion are nearly identical, consistent with their isoelectric properties. The −O−, −S−, and −NH insertion reduced the VB edge state by eliminating the In−Ga metallic bonds. However, the edge As atoms still have nontetrahedral bond angles (red arrows), consistent with negligible reduction in the CB edge state density.

To test if a different bonding angle might influence the CB edge states, DFT was employed to model −OH, −SH, and $-NH_2$ insertion into the metallic bonds, as shown in Figure 3. Note that all three ligands give nearly identical electronic structures. These hydride insertion results have a less passivating effect on the VB edge states compared to simple atomic insertion, but there is partial passivation of the CB edge states. The DFT structural model shows the cause of the CB edge state partial passivation. Although pairs of −OH, −SH, and $-NH_2$ groups were inserted into the metal−metal bonds, DFT relaxation resulted in one of the hydride groups moving out of the metal−metal bond and eliminating a dangling bond of one of the tricoordinated In/Ga atoms. This configuration satisfies the electron-counting model, whereas having two bridging oxidant groups or two edge oxidant groups leads

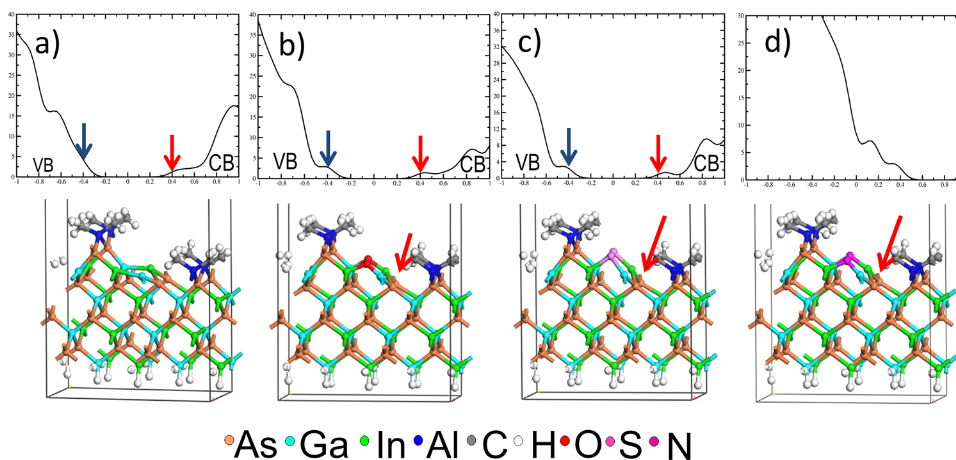

Figure 2. Side view of relaxed DFT models and DOS of TMA passivated (2 × 4) surface (a) with an O atom (b), S atom (c), and N atom (d) inserted between group III atoms. Note that the electronic structures for passivation with O and S are nearly identical. Both reduce the VB edge state by eliminating the In–Ga metallic bonds. However, the edge As atoms (arrow) still have nontetrahedral bond angles. The N passivation leaves the edge As atoms with highly distorted bond angles (arrow) and half-filled dangling bonds on N atoms which pin the Fermi level.

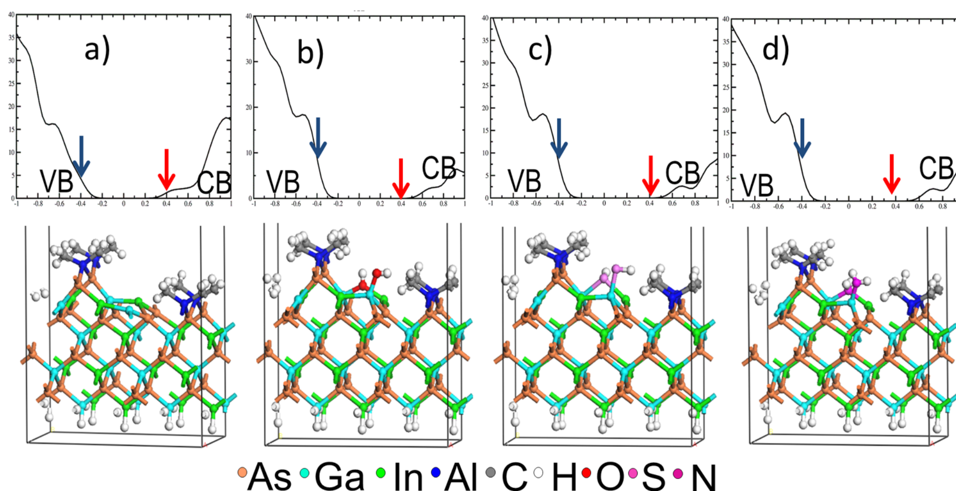

Figure 3. Side view of relaxed DFT models and DOS of TMA passivated (2 × 4) surface (a) with an –OH group (b), –SH group (c), and $-NH_2$ group (d) inserted between group III atoms. Note that the electronic structures for passivation with –OH, –SH, and $-NH_2$ are nearly identical. In all cases, one-half of the ligands migrated out of the In–Ga bonds to passivate a Ga dangling bond, resulting in an increase of VB edge states and a decrease of CB edge states. All cases reduced the CB edge state by eliminating the In–Ga metallic bonds and partially relieving bond angle strain in the edge As atoms.

to excess charge or a charge deficiency, respectively. The lack of passivation of the VB edge states is consistent with one of the metal–metal bonds remaining intact, while the partial passivation of the CB edge state is consistent with the dangling bonds on the tricoordinated In/Ga atoms being a source of the bond angle strain which induced CB edge states. As shown in Figure 1, the empty dangling bonds on the tricoordinated In/Ga atoms do not directly induce CB edge states; instead, they induce bond angle strain on the neighboring As atoms (red arrows), which causes the CB edge states.

To eliminate both the metal–metal bonds and the group III dangling bonds in the DFT model, –OH, –SH, or $-NH_2$ groups were inserted into the metallic bonds and bonded to the edge tricoordinated In/Ga atoms. Note that all three ligands give nearly identical electronic structures. One of the methyl groups from the DMA molecule migrated and bonded to the left surface Ga atom. This configuration satisfies the electron-counting rule and results in a neutral unit cell. Additionally, this double passivation restored the edge As atom bond angles to sp^3 tetrahedral geometry with an angle much closer to the ideal 109.5°, and the CB edge states were completely suppressed as shown in Figure 4b–d. The models are consistent with the effect of dual passivation: a reductant (TMA) is used to eliminate the dangling bonds on the tricoordinated As atoms, while an oxidant (–OH, –SH, or $-NH_2$) is used to eliminate both the metal–metal bonds and the group III dangling bonds.

STM/STS. After the sample was decapped, STM was used to verify that the InGaAs (001)-(2 × 4) surface was free of contaminants (Figure 5a). The zigzag pattern of

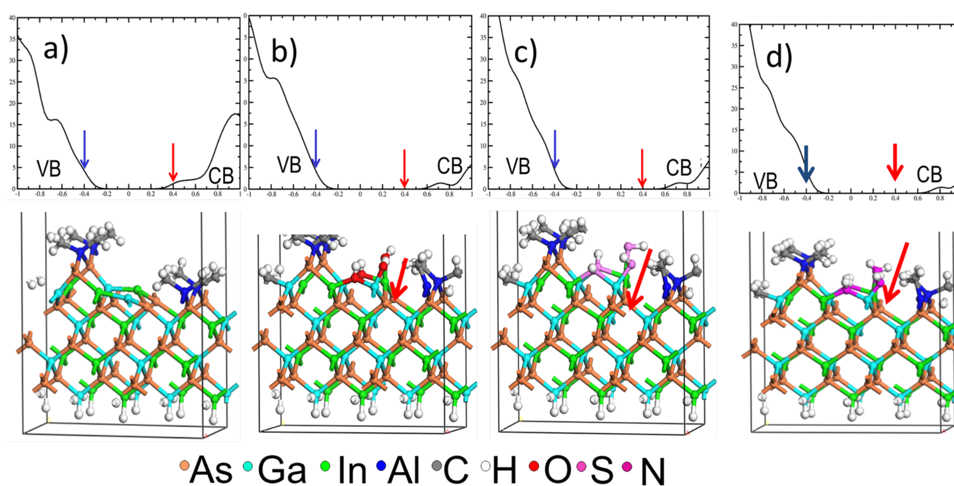

Figure 4. Side view of relaxed DFT models and DOS of TMA passivated (2 × 4) surface (a) with two −OH groups (b), −SH groups (c), and $-NH_2$ groups (d) inserted between group III atoms and on the edge of group III atoms. The electronic structures for passivation with −OH, −SH, and $-NH_2$ are nearly identical. The ligands have removed the dangling bonds on the In and Ga atoms, resulting in the edge As atoms (arrows) being restored to bulk-like tetrahedral bonding angles, which eliminates the CB edge states.

the rows in the STM image is due to the presence of two different unit cells on the (2 × 4) surface, the α2-(2 × 4) and the β2-(2 × 4) unit cells.[12] Details of the different unit cells are given in a previous study which has shown that $In_{0.27}Ga_{0.73}As$ contains 42% missing dimer unit cells and $In_{0.53}Ga_{0.47}As$ has 78%.[11] DFT simulations (Figures 1−4) show that the defect unit cells cannot be fully passivated by TMA and require an oxidizing agent to suppress the remaining CB edge states. Two passivation experiments were performed to achieve dual passivation.

In the first experiment, 1000 L of HOOH vapor was dosed onto the clean (2 × 4) surface at 25 °C and was followed by anneals at 210, 250, 350, and 410 °C, each for 30 min. A STM image of the final surface is shown in Figure 5b. By manually counting the number of α2-(2 × 4) unit cells in the STM image, it was determined that the percentage of α2-(2 × 4) unit cells was decreased from 78 to 24%, consistent with selective insertion of −OH groups into the metallic group III bonds. The HOOH dosed InGaAs (001)-(2 × 4) sample was subsequently annealed to 460 °C for an additional 30 min, as shown in Figure 5c. The characteristic zigzag pattern of the clean surface is visible, indicating that the adsorption of −OH is reversible and there is no subsurface oxidation for low-temperature dosing even with a high-temperature anneal since this would irreversibly change the surface structure. In a separate experiment, 3000 L of HOOH was dosed followed by the same series of anneals in an attempt to reduce the number of α2 unit cells. No high-resolution images were obtained after several days of scanning. It is believed that the oxidant was regularly reacting with the tip, effectively limiting the resolution of the image.

Figure 6 shows a sample that was initially dosed with 1500 L of HOOH, annealed to 320 °C, and subsequently dosed with 500 L of TMA at 25 °C and annealed to 280 °C. The HOOH dosing is manually controlled, hence the variation in total dose between Figure 5 and Figure 6 is limited by the ability to control the extent of manual dosing in real time. There are atomically ordered rows in the $(\bar{1}10)$ direction with row spacing of 1.68 ± 0.09 nm, the same as the clean (2 × 4) surface (Figure 6 inset). This suggests the lack of subcutaneous oxidation, but the zigzag pattern observed for both the clean (2 × 4) surface and the TMA-only dosed surface is not visible, indicating preferential insertion of the −OH groups into the metallic bonds.[22] Growth of Al_2O_3 has been nucleated in each unit cell because the TMA selectively reacted with the As−As dimers and the HOOH reacted with the group III bonds.

An STS study was performed to determine the effects of dosing TMA only (green curve), HOOH only (red curve), and dual passivation with HOOH and TMA (pink curve) (Figure 7). The E_f, defined as the 0 V position in STS, is located near the CB edge for the clean surface (blue curve), meaning the E_f is unpinned. Previous studies on clean n-type and p-type InGaAs (2 × 4) and on TMA dosed n-type and p-type InGaAs (2 × 4) demonstrated that the E_f remained near the VB for p-type samples and near the CB for n-type samples, indicating an unpinned Fermi level.[22] After being dosed with 1000 L of TMA (green curve) at 280 °C with a 280 °C anneal, the E_f shifts slightly toward midgap, indicating a partially pinned surface. After the clean (2 × 4) surface was dosed with 1000 L of HOOH (g) (red curve) at 25 °C with a 310 °C anneal, the Fermi level position remains unchanged from the clean surface position, which is in contrast to several publications, indicating that oxidant dosing of III−V surfaces results in a pinned E_f.[6,23−25] Dosing 1000 L of HOOH at 25 °C with a 300 °C anneal and subsequently 1000 L of TMA at 280 °C followed by an anneal at 280 °C for 30 min (pink) results in further unpinning of the E_f when

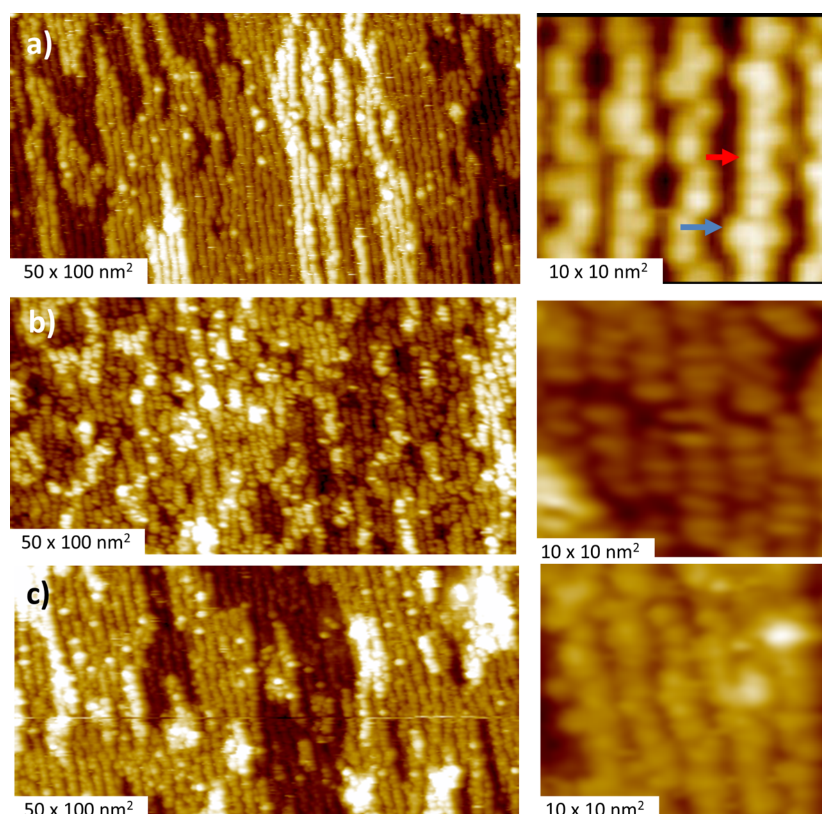

Figure 5. (a) Filled state STM images of a clean (2 × 4) surface with a β2 double As dimer unit cell (blue arrow) and an α2 single As dimer unit cell (red arrow). (b) A 1000 L dose of HOOH followed by a series of anneals; notice that a majority of unit cells appear wide, indicating selective insertion of –OH groups into the metallic In–Ga bond. (c) Same sample after annealing up to 460 °C; notice the restoration of the characteristic zigzag pattern indicating reversible chemisorption of –OH groups on the (2 × 4) surface.

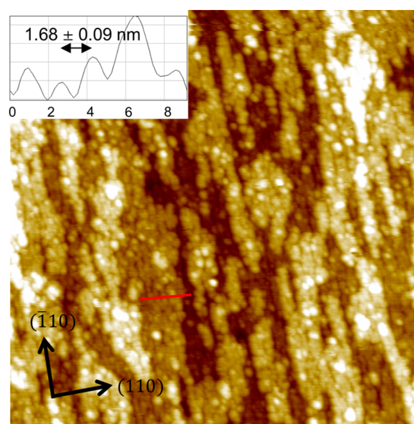

Figure 6. STM image of a 100 × 100 nm^2 filled state of the InGaAs (2 × 4) surface initially dosed with HOOH and subsequently dosed with TMA. Ordered rows appear in the vertical direction, indicating that a high degree of surface order is maintained (inset), but the zigzag pattern of a typical (2 × 4) surface is not observed, indicating selective insertion of –OH groups into metallic In–Ga bonds. Al_2O_3 ALD is nucleated in each unit cell since TMA reacted with As dimers and –OH groups reacted with In/Ga atoms.

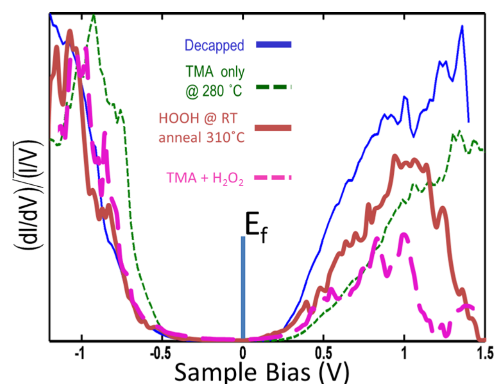

Figure 7. STS spectra of the clean (2 × 4) surface (blue) showing the Fermi level near the CB edge, indicating an unpinned Fermi level, the TMA dosed surface (green) which shows a slight shift of Fermi level toward midgap due to unpassivated metallic bonds, the HOOH dosed surface (red) which is nearly identical to the clean surface, and the TMA + HOOH dosed surface (pink) which has a Fermi level near the CB edge, consistent with unpinning.

compared to the TMA-only dose. Although the DFT calculations showed that reacting the clean (2 × 4) surface with both TMA and –OH groups should passivate CB edge states, this experiment shows that dosing both TMA and HOOH does not completely unpin the Fermi level. To achieve a fully unpinned surface E_f, it may be necessary to decrease the number of α2-(2 × 4) unit cells below 23% by further optimizing the dosing conditions. However, in gate oxide

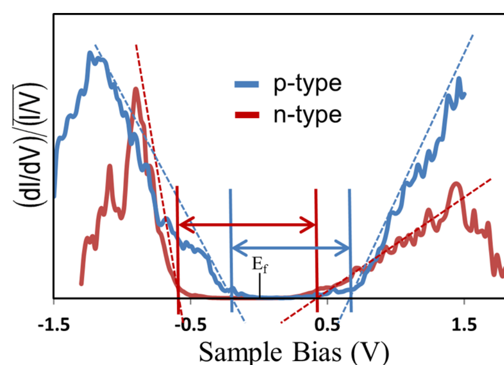

Figure 8. (Red curve) STS of n-type InGaAs dosed with 1000 L of HOOH followed by 1000 L of TMA. To ensure the E_f is fully unpinned, p-type InGaAs was dosed with 1000 L HOOH and 1000 L of TMA. E_f is clearly located near the VB for the p-type sample, indicative of unpinning.

deposition, there will be subsequent exposure to H_2O during ALD, which is likely to remove most remaining metal–metal bonds. To ensure that the E_f was not pinned near the CB due to In surface segregation,[26] n-type and p-type samples were compared (Figure 8). A p-type sample was dosed with 1000 L of HOOH at 25 °C and subsequently dosed with 1000 L of TMA at 280 °C. The E_f is located near the VB for the p-type sample and near the CB for the n-type sample, indicating that the E_f is not pinned near the CB.

CONCLUSION

This study has identified the physical origins of electronic trap states present at the InGaAs/oxide interfaces and presented an effective dual passivation scheme using an oxidant and a reductant which eliminates metallic bonds, dangling bonds, and dangling-bond-induced strain. Employing this passivation technique will result in superior electrical performance due to suppression of electronic defects and is applicable to a wide range of devices containing compound semiconductor/oxide junctions.

METHODS

The samples contained 0.2 μm of molecular beam epitaxy grown $In_{0.53}Ga_{0.47}As$ (001) with 1×10^{18} cm^{-3} Si dopant concentrations on commercially available InP wafers. The samples were capped with ~50 nm of As_2 to protect the InGaAs surface from contaminants and oxidation. Samples were loaded into an Omicron variable-temperature ultrahigh vacuum system with a base pressure of <1×10^{-10} Torr. The As_2 cap was thermally desorbed at 350 °C, and the (2 × 4) surface reconstructions were obtained by annealing the samples to 400 °C. Samples were transferred *in situ* to the scanning probe microscopy chamber with a base pressure of 1×10^{-11} Torr, where STM and STS were performed on the clean (2 × 4) surfaces. STM experiments were performed in constant current mode with a sample bias of −3 V and a tunneling current set point of 100 pA. All images have been reproduced at least twice. The distance between rows was determined by averaging 10 separate line traces and calculating the standard error. STS was performed in varied-*z* mode while ramping the sample bias from −1.5 to 1.5 V and concurrently moving the tip toward then away from the surface. All STS curves are an average of at least eight individual curves. After being dosed with TMA and/or an oxidant, STM was used to determine the atomic configuration of the surface while STS was used to measure the electrical quality of the surface.[3,27,28] Specific dosing conditions for each experiment are given in the corresponding results section.

All DFT calculations were performed with the Vienna Ab Initio Simulation Package[29,30] using projector-augmented wave (PAW) pseudopotentials (PP)[31] and the PBE (Perdew–Burke–Ernzerhof) exchange-correlation functional.[32,33] The choice of PBE functional and PAW PPs was validated by parametrization runs that demonstrated good reproducibility of experimental lattice constants, bulk moduli, and formation energies for bulk crystalline GaAs and InAs. The three bottom layers of InGaAs were permanently fixed in their bulk-like positions and passivated by pseudo-H atoms with 1.25 $|e|$ charge to simulate continuous bulk. The systems were DFT-relaxed by a conjugate-gradient geometry optimization algorithm with a force tolerance level of 0.05 eV/Å at the $4 \times 8 \times 1$ Γ-centered K-point set.

Conflict of Interest: The authors declare no competing financial interest.

Acknowledgment. This work was supported by the Semiconductor Research Corporation.

Supporting Information Available: The supporting material addresses a few key issues including the possibility of utilizing H_2O as the oxidant and the temperature dependence of this passivation, proving the E_f is truly unpinned and located near the CB and not pinned near the CB due to In surface segregation, the effect of In/Ga ordering on the DOS, identifying the bulk *vs* surface states, and exploring alternate bonding configurations of the oxidant species. This material is available free of charge *via* the Internet at http://pubs.acs.org.

REFERENCES AND NOTES

1. Künzel, H.; Böttcher, J.; Gibis, R.; Urmann, G. Material Properties of $Ga_{0.47}In_{0.53}As$ Grown on InP by Low-Temperature Molecular Beam Epitaxy. *Appl. Phys. Lett.* **1992**, *61*, 1347–1349.
2. Gill, D. M.; Kane, B.; Svensson, S. P.; Tu, D.; Uppal, P.; Byer, N. High-Performance, 0.1 μm InAlAs/InGaAs High Electron Mobility Transistors on GaAs. *IEEE Electron Device Lett.* **1996**, *17*, 328–330.
3. Mönch, W. *Semiconductor Surfaces and Interfaces*; Springer Science & Business Media: Berlin, 2001; pp 1–7.
4. Wilks, S. Engineering and Investigating the Control of Semiconductor Surfaces and Interfaces. *J. Phys. D: Appl. Phys.* **2002**, *35*, R77–R90.
5. Hasegawa, H.; Negoro, N.; Kasai, S.; Ishikawa, Y.; Fujikuwa, H. Effects of Gap States on Scanning Tunneling Spectra Observed on (110) and (001) Oriented Clean Surfaces and Ultrathin Si Layer Covered Surfaces of GaAs Prepared by Molecular Beam Epitaxy. *J. Vac. Sci. Technol., B* **2000**, *18*, 2100–2108.
6. Spicer, W.; Chye, P.; Garner, C.; Lindau, I.; Pianetta, P. The Surface Electronic Structure of 3–5 Compounds and the Mechanism of Fermi Level Pinning by Oxygen (Passivation) and Metals (Schottky Barriers). *Surf. Sci.* **1979**, *86*, 763–788.
7. Petroff, P. Transmission Electron Microscopy of Interfaces in III–V Compound Semiconductors. *J. Vac. Sci. Technol., A* **1977**, *14*, 973–978.
8. Ye, P. D. Main Determinants for III–V Metal-Oxide-Semiconductor Field-Effect Transistors. *J. Vac. Sci. Technol., A* **2008**, *26*, 697–704.
9. Robertson, J. Model of Interface States at III–V Oxide Interfaces. *Appl. Phys. Lett.* **2009**, *94*, 152104.
10. Hwang, Y.; Engel-Herbert, R.; Stemmer, S. Influence of Trimethylaluminum on the Growth and Properties of

$HfO_2/In_{0.53}Ga_{0.47}As$ Interfaces. *Appl. Phys. Lett.* **2011**, *98*, 052911.
11. Edmonds, M.; Melitz, W.; Kent, T.; Chagarov, E.; Kummel, A. C. Surface Preparation and In/Ga Alloying Effects on InGaAs (001)-(2 × 4) Surfaces for ALD Gate Oxide Deposition. *ECS Trans.* **2012**, *50*, 129–140.
12. Shen, J.; Winn, D. L.; Melitz, W.; Clemens, J. B.; Kummel, A. C. Real Space Surface Reconstructions of Decapped As-Rich $In_{0.53}Ga_{0.47}As$ (001)-(2× 4). *ECS Trans.* **2008**, *16*, 463–468.
13. Lamagna, L.; Fusi, M.; Spiga, S.; Fanciulli, M.; Brammertz, G.; Merckling, C.; Meuris, M.; Molle, A. Effects of Surface Passivation during Atomic Layer Deposition of Al_2O_3 on $In_{0.53}Ga_{0.47}As$ Substrates. *Microelectron. Eng.* **2011**, *88*, 431–434.
14. Besser, R.; Helms, C. Comparison of Surface Properties of Sodium Sulfide and Ammonium Sulfide Passivation of GaAs. *J. Appl. Phys.* **1989**, *65*, 4306–4310.
15. Alian, A.; Brammertz, G.; Merckling, C.; Firrincieli, A.; Wang, W.; Lin, H. C.; Caymax, M.; Meuris, M.; De Meyer, K.; Heyns, M. Ammonium Sulfide Vapor Passivation of $In_{0.53}Ga_{0.47}As$ and InP Surfaces. *Appl. Phys. Lett.* **2011**, *99*, 112114.
16. Bessolov, V.; Lebedev, M. Chalcogenide Passivation of III–V Semiconductor Surfaces. *Semiconductors* **1998**, *32*, 1141–1156.
17. Capasso, F.; Williams, G. A Proposed Hydrogenation/Nitridization Passivation Mechanism for GaAs and Other III–V Semiconductor Devices, Including InGaAs Long Wavelength Photodetectors. *J. Electrochem. Soc.* **1982**, *129*, 821–824.
18. Feenstra, R. M.; Stroscio, J. A.; Tersoff, J.; Fein, A. Atom-Selective Imaging of the GaAs (110) Surface. *Phys. Rev. Lett.* **1987**, *58*, 1192–1195.
19. Feenstra, R. M.; Meyer, G.; Moresco, F.; Rieder, K. H. Low-Temperature Scanning Tunneling Spectroscopy of n-Type GaAs(110) Surfaces. *Phys. Rev. B* **2002**, *66*, 165204.
20. Kent, T. J.; Edmonds, M.; Chagarov, E.; Droopad, R.; Kummel, A. C. Dual Passivation of GaAs (110) Surfaces Using O_2/H_2O and Trimethylaluminum. *J. Chem. Phys.* **2013**, *139*, 244706.
21. Hinkle, C.; Sonnet, A. M.; Vogel, E. M.; McDonnell, S.; Hughes, G. J.; Milojevic, M.; Lee, B.; Aguirre-Tostado, F. S.; Choi, K. J.; Kim, H. C.; Kim, J.; Wallace, R. M. GaAs Interfacial Self-Cleaning by Atomic Layer Deposition. *Appl. Phys. Lett.* **2008**, *92*, 071901.
22. Melitz, W.; Kent, T.; Droopad, R.; Holland, M.; Thayne, I.; Kummel, A. C. Atomic Imaging of Atomic Layer Deposition Oxide Nucleation with Trimethylaluminum on As-Rich InGaAs(001) 2 × 4 *vs* Ga/In-Rich InGaAs(001) 4 × 2. *J. Chem. Phys.* **2012**, *136*, 154706.
23. Spicer, W.; Chye, P.; Skeath, P.; Su, F. C.; Lindau, I. New and Unified Model for Schottky Barrier and III–V Insulator Interface States Formation. *J. Vac. Sci. Technol.* **1979**, *16*, 1422–1433.
24. Spicer, W. E.; Lindau, I.; Skeath, P.; Su, C. Y.; Chye, P. Unified Mechanism for Schottky-Barrier Formation and III–V Oxide Interface States. *Phys. Rev. Lett.* **1980**, *44*, 420–423.
25. Hale, M. J.; Yi, S. I.; Sexton, J. Z.; Kummel, A. C.; Passlack, M. Scanning Tunneling Microscopy and Spectroscopy of Gallium Oxide Deposition and Oxidation on GaAs(001)-c(2 × 8)/(2 × 4). *J. Chem. Phys.* **2003**, *119*, 6719–6728.
26. Hasegawa, H.; Ohno, H. Unified Disorder Induced Gap State Model for Insulator–Semiconductor and Metal–Semiconductor Interfaces. *J. Vac. Sci. Technol., B* **1986**, *4*, 1130–1138.
27. Feenstra, R. M. Scanning Tunneling Spectroscopy. *Surf. Sci.* **1994**, *299*, 965–979.
28. Stroscio, J. A.; Feenstra, R.; Newns, D.; Fein, A. Voltage-Dependent Scanning Tunneling Microscopy Imaging of Semiconductor Surfaces. *J. Vac. Sci. Technol., A* **1988**, *6*, 499–507.
29. Kresse, G.; Furthmüller, J. Efficiency of *Ab Initio* Total Energy Calculations for Metals and Semiconductors Using a Plane-Wave Basis Set. *Comput. Mater. Sci.* **1996**, *6*, 15–50.
30. Kresse, G.; Furthmüller, J. Efficient Iterative Schemes for *Ab Initio* Total-Energy Calculations Using a Plane-Wave Basis Set. *Phys. Rev. B* **1996**, *54*, 11169.
31. Perdew, J. P.; Burke, K.; Ernzerhof, M. Generalized Gradient Approximation Made Simple. *Phys. Rev. Lett.* **1996**, *77*, 3865–3868.
32. Blochl, P. E. Projector Augmented-Wave Method. *Phys. Rev. B* **1994**, *50*, 17953.
33. Kresse, G.; Joubert, D. From Ultrasoft Pseudopotentials to the Projector Augmented-Wave Method. *Phys. Rev. B* **1999**, *59*, 1758–1775.